UNIVERSITY OF LEEDS

Article:
Semprini, M, Cuppone, AV, Delis, I et al. (3 more authors) (2017) Biofeedback Signals for Robotic Rehabilitation: Assessment of Wrist Muscle Activation Patterns in Healthy Humans. IEEE Transactions on Neural Systems and Rehabilitation Engineering, 25 (7). pp. 883-892. ISSN 1534-4320

https://doi.org/10.1109/TNSRE.2016.2636122

Biofeedback Signals for Robotic Rehabilitation: Assessment of Wrist Muscle Activation Patterns in Healthy Humans

Marianna Semprini, Anna Vera Cuppone, Ioannis Delis, Valentina Squeri, Stefano Panzeri, and Jürgen Konczak

Abstract— Electrophysiological recordings from human muscles can serve as control signals for robotic rehabilitation devices. Given that many diseases affecting the human sensorimotor system are associated with abnormal patterns of muscle activation, such biofeedback can optimize human-robot interaction and ultimately enhance motor recovery. To understand how mechanical constraints and forces imposed by a robot affect muscle synergies, we mapped the muscle activity of 7 major arm muscles in healthy individuals performing goal-directed discrete wrist movements constrained by a wrist robot. We tested 6 movement directions and 4 force conditions typically experienced during robotic rehabilitation. We analyzed electromyographic (EMG) signals using a space-by-time decomposition and we identified a set of spatial and temporal modules that compactly described the EMG activity and were robust across subjects. For each trial, coefficients expressing the strength of each combination of modules and representing the underlying muscle recruitment, allowed for a highly reliable decoding of all experimental conditions. The decomposition provides compact representations of the observable muscle activation constrained by a robotic device. Results indicate that a low-dimensional control scheme incorporating EMG biofeedback could be an effective add-on for robotic rehabilitative protocols seeking to improve impaired motor function in humans.

Index Terms— Biofeedback, electromyography, muscle synergies, robotic rehabilitation.

I. INTRODUCTION

Robotic rehabilitation has been proposed as a valuable tool to aid the recovery of motor function after neurological damage [1]. Several approaches on how best to control robotic assistive devices have been described. Traditionally, such assistance is based on the subject's ability to voluntarily control movements [2]. More recently, biofeedback from the user has been included into rehabilitative protocols and in these cases electromyographic (EMG) signals were typically employed and displayed to the subject as visual feedback [3]. Previous research demonstrated the advantage of biofeedback in suppressing abnormal muscle activation and promoting motor recovery [4], and consequently the incorporation of biofeedback has been promoted for robotic rehabilitation [5-7]. However, when considering the interaction of a human patient with a rehabilitation robotic device, muscle activation patterns are going to be different from the activation patterns during functional and unconstrained movements. We have advocated that such differences should be taken into account when designing a rehabilitation protocol that includes the use of biofeedback [8]. Moreover, EMG signals of neurologic patients show a wide range of abnormalities due to the underlying pathophysiology and the larger between-patient variability inherent to disease states [9]. When designing a rehabilitation protocol, it is therefore necessary to take into account the differences in muscular activation due to the human-robot interaction together with the known electrophysiological abnormalities of the EMG signals associated with the disease.

In order to use such biofeedback signals during robotic rehabilitation of patients that are known to have abnormalities in muscular activation, it is paramount to document in detail the patterns of EMGs in healthy subjects using robotic rehabilitation devices. Once the characteristic patterns of muscle activation imposed by a robotic rehabilitation device are known, these patterns can be used to produce standardized muscle innervation profiles for each task in which a patient shall engage as part of a rehabilitation protocol. That, in turn, will allow to quantify the degree of abnormality for each patient as the difference between a prototypical and a pathological EMG signal.

Because such prototypical muscle activation profiles for robot-constrained interactions are largely not available, we here study muscular synergistic control during human-robot interaction by mapping the EMG patterns of healthy adults interacting with a wrist robotic device. We tested 12 healthy subjects performing goal-directed wrist movements using a 3 degrees-of-freedom (DoFs) wrist robot. Simultaneously, we recorded EMG activity of 7 major arm and forearm muscles that rotate the wrist/hand complex in each of its three DoFs (flexion/extension, abduction/adduction, and supination/pronation). For each subject we extracted the underlying modules of muscle

M.S. and S.P. are with the Neural Computation Laboratory, Istituto Italiano di Tecnologia, Rovereto, Italy (e-mails: marianna.semprini@iit.it, stefano.panzeri@iit.it).

A.V.C. and V.S. are with the Robotics Brain and Cognitive Science Department, Istituto Italiano di Tecnologia, Genova, Italy (e-mails: anna.cuppone@iit.it, valentina.squeri@iit.it).

I.D. is with the Department of Biomedical Engineering, Columbia University, New York, NY 10027, USA, (e-mail: ioannis.delis@columbia.edu).

J.K. is with the Human Sensorimotor Control Lab, Center for Clinical Movement Science and School of Kinesiology, University of Minnesota, USA, (e-mail:jkonczak@umn.edu).

activity using a novel space-by-time decomposition method [10] and then averaged them across subjects in order to obtain the typical temporal and spatial muscle activation patterns constrained by robotic devices. Finally, this analysis allowed representing each EMG signal as a set of coefficients in the modular space.

II. MATERIALS AND METHODS

A. Participants

12 right-handed subjects (age: 29 ± 4 years) with no known neuromuscular disorders and naïve to the tasks participated to the study. All participants gave their informed consent prior to testing. The study was approved by the local ethics committee, Comitato Etico of the ASL3 of Genova (Italy).

B. Experimental Setup

The robotic device was a wrist robot and consisted of a completely back drivable manipulandum with 3 DoFs [11]. The robot was powered by 4 brushless motors that provide an accurate haptic rendering and compensate for the weight and inertia of the device. Displacement at each DoF was measured by means of a high-resolution incremental optical encoder (2048 bits/rev). The haptic robot could apply forces during task execution (running frequency 1 kHz). The system was integrated with a virtual reality environment that runs at 60 Hz and represented the visual feedback to the subject during the motor tasks. A computer screen, positioned in front of the subject about 1 m away, displayed the current positions of hand and target. Fig. 1 shows the experimental setup.

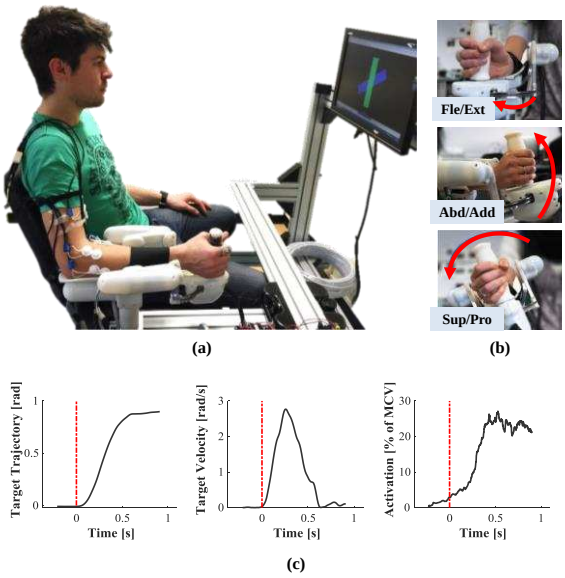

Fig. 1: Experimental setup. (a) Participants placed the wrist on the wrist robot and grasped the robot handle. Surface EMG electrodes were placed on the arm and forearm. A computer screen displayed the target and the wrist end effector position. (b) Robot allowed movements along three different DoFs: flexion/extension (top), abduction/adduction (middle) and pronation/supination (bottom). Fle = flexion, Ext = extension, Abd = abduction, Add = adduction, Sup = supination, Pro = pronation. (c) Typical recording of one single subject during extension: left panel shows 1 DoF target trajectory, middle panel target velocity and right panel EMG activation of Flexor Carpi Ulnaris muscle aligned in time; red dashed lines indicate target onset.

The robot system communicated with the EMG acquisition system (EMG USB2 OT BIOelettronica 64 channels) using an Analog and Digital I/O PCI card (Sensoray, 626) that allowed the robot to send a digital signal to the EMG system in such a way as to synchronize the two systems. During recording, the EMG acquisition system was battery-powered in order to avoid electrical-supply noise. The raw EMG signals were sampled at 2048 Hz sampling rate with selectable amplification gain and high-/low-pass bandwidths. For EMG signals acquisition during the task execution, we selected a gain of 2000. While collecting for maximum voluntary contraction (MVC) data the gain was set to 1000, in order to avoid signal saturation.

C. Experimental Protocol

Participants sat on a chair, placed their right arm on the support of the robot and grabbed the end effector (Fig. 1). Subjects performed a center-out task with their wrist in one of the three DoFs, Flexion-Extension (FE), Abduction-Adduction (AA) and Pronation-Supination (PS). The task consisted of a sequence of 6 discrete movements: wrist flexion, extension, abduction, adduction, and forearm pronation and supination. Subjects were restricted to move only along one DoF per movement with the other DoFs being dynamically blocked by the robot. Each movement was repeated 5 times, without any time constraint. Subjects received visual feedback about the current wrist position. On a computer screen movement along FE was visualized as a linear movement of a cursor on the x-axis, AA on the y-axis and PS as a rotation around the z-axis; the target and end effector were displayed as round circles (2 cm diameter) in FE and AA movements and as two vertical bars (2x5 cm^2) of different colors during PS movements. The reaching task was executed in a workspace considering the 75% of the joint maximum active range of motion (RoM) in heathy adults, which we approximated to be respectively equal to ±70° for flexion and extension, ±20° for abduction and adduction and ±80° for pronation and supination [12]. The 0° corresponded to the central position where the robot axes are aligned with the wrist rotational axis.

The above protocol was repeated under 4 different task conditions, differing on the force level applied by the robot: Null Field, Resistive Field (field of constant force opposite to the target direction), Assistive Field (field of constant force in target direction) and Passive Field (the robot moves the target end effector while subject closed the eyes). In Resistive and Assistive Field condition the amount of constant force was the same but the direction was opposite (against target movement in the Resistive Field condition) and it corresponded to the 70% of a maximum torque used in the Passive condition. Equation (1) describes the applied force:

$$F = \pm 0.7 * k * d * \frac{(X_{EE} - X_{TG})}{|X_{EE} - X_{TG}|} \qquad (1)$$

, where k = 0.3 N·m/rad in FE and PS movements and 0.6 N·m/rad in AA movements), d = 0.05 rad, X_{EE} is the position of the end effector and X_{TG} the position of the target.

In the Passive Field condition, we used an elastic force proportional to the distance between the end effector and a

TABLE I
RECORDED MUSCLES AND THEIR ACTION.

Muscle	Action
Flexor Carpi Radialis (FCR)	Wrist flexion, abduction
Flexor Carpi Ulnaris (FCU)	Wrist flexion, adduction
Extensor Carpi Radialis (ECR)	Wrist extension, abduction
Extensor Carpi Ulnaris (ECU)	Wrist extension, adduction
Biceps Brachii (BIC)	Shoulder and elbow flexion
Brachioradialis (BR)	Elbow flexion, forearm supination or pronation
Pronator Teres (PT)	Forearm pronation

List of the recorded muscles and the associated joint movement during concentric muscle contraction.

moving target from the initial position and the final position, expressed by equation (2):

$$F = k\ (X_{EE} - X_{TG}) \qquad (2)$$

, where k = 0.3 N·m/rad. In this case, the target moved along a minimum jerk trajectory.

EMG surface electrodes (Ag/AgCl with a diameter of 26 mm) were placed on the arm and forearm with a center distance less than 2 cm to record the activity of 7 muscles involved in wrist movement. EMG recording was performed in single differential mode. Correct electrode placement was verified by observing the activation of each muscle during specific movements known to involve it [12]. During this procedure, EMG signals were monitored in order to optimize recording quality and minimize cross-talk from adjacent muscles during isometric contractions. TABLE I lists the muscles we recorded from and the movement involving them.

D. Extraction of Synergistic EMG Activation Patterns

To extract invariant activation patterns (or "modules") of muscle activity from the EMG recordings we used a Non-Negative Matrix Factorization (NMF) method factorizable in space and time, which we call the space-by-time NMF decomposition [13, 14]. This method decomposes the original dataset into N non-negative spatial modules (describing the stereotypical patterns of simultaneous EMG activations of groups of muscles) and P non-negative temporal modules (describing the stereotypical patterns of activation over time of these groups of muscles) such that single trial EMG recordings can be represented as a set of $N \times P$ non-negative activation coefficients describing the strength of recruitment of each of these modules in each single trial. The decomposition is defined by the following equation:

$$\boldsymbol{m^s}(\mathrm{t}) = \sum_{i=1}^{P}\sum_{j=1}^{N} w_i(t)\, a_{ij}^{s}\boldsymbol{w_j} + residual \qquad 3)$$

, where $\boldsymbol{m^s}(\mathrm{t})$ denote the EMG dataset, $1 > s > S$ is the number of samples (S being the total number of samples), $1 > t > T$ is the number of discrete time frames (T = 1000 in our implementation), $w_i(t)$ are the temporal modules, $\boldsymbol{w_j}$ are the spatial modules, a_{ij} are the activation coefficients and $residual$ indicates the reconstruction error. The decomposition algorithm uses an iterative procedure based on multiplicative update rules that minimize the total reconstruction error, therefore the algorithm is guaranteed to converge to a local minimum. The optimization problem is not convex, so the local minimum is not necessarily global. This also implies that the modules found are not unique. To address this, here for each module extraction we ran the algorithm 10 times and chose the decomposition that gave the lowest reconstruction error. Empirically, however, the modules were almost identical from one algorithm run to the next, which suggests that even one algorithm run would be sufficient to yield the reported results.

Before applying the space-by-time NMF decomposition, EMG data were preprocessed as follows. EMG signals were filtered offline with a 6th order Butterworth band pass filter between 30 and 400 Hz, subsequently rectified and smoothed with a moving average filter using a window length of 150 ms. The filtered EMG was scaled by the relative maximum voluntary contraction (MVC) value, enabling inter-subjects comparison of EMG data. We considered the portion of signal from target onset to target reach and resampled each signal using a linear interpolation for T = 1000 frames.

1) Assessment of Extracted Modular Decompositions

To evaluate the quality of the resulting modular decompositions, we quantified a) how well they approximated the original EMG recordings by computing the Variance Accounted For and b) how well they discriminated the performed motor tasks in single trials by computing single-trial task decoding performance [10, 15].

The modular decomposition should approximate the recorded EMG signals as accurately as possible. To quantify this, we computed the Variance Accounted For (VAF) which evaluates the quality of reconstruction of the original EMG data from the modular decomposition. Here, following [16], VAF was defined as the total approximation error divided by the total variance of the dataset. The VAF indicates how well the EMG data can be reconstructed by combining modules and activation coefficients, e.g. if VAF = 0.9 then 90% of the original EMG data are reconstructed.

Importantly, we aimed to identify the modular decomposition that explained the highest proportion of task-related variability in muscle activity. To quantify this, we computed the single-trial task decoding metric. We used as decoding parameters the activation coefficients of the modular decomposition, which encode the level of activation of spatial and temporal modules in individual trials. Specifically, task decoding was performed using the activation coefficients a_{ij}^{s} as input to a linear discriminant algorithm (LDA) combined with a leave-one-out cross-validation procedure [13]. Decoding performance (DEC) was measured as the percentage of correctly decoded trials (% correct). Given that 6 movement directions were tested under 4 different force conditions, the total number of experimental conditions was $K = 6 \times 4 = 24$ and the chance level of the decoder was $1/K = 0.041$. Hence, a decoding performance value greater than 0.041 indicated that the decoder reliably discriminated across conditions. We assessed the statistical significance of decoding performance using the Bernoulli test [17]. In brief,

assuming each stimulus as a sequence of Bernoulli trials (independent trials with two possible outcomes: success and failure), the probability of successes follows the Binomial distribution. Hence, the p-value of K successes is computed by adding the probabilities of getting K or more successes by chance.

2) Selecting the Number of Modules in the space-by-time NMF decomposition

Given that the number of spatial and temporal modules was not known a priori, we iteratively ran the space-by-time decomposition method assuming all possible combinations of P temporal and N spatial modules, with $N, P = 1 \div 7$. We chose 7 as the maximum number of modules given that we recorded from 7 muscles (7 temporal and 7 spatial modules would potentially capture the activation pattern of each individual muscle).

In order to establish the minimal number of modules capturing all the task-discriminating variability of the dataset, we computed a joint metric incorporating both VAF and decoding performance ($VDM = DEC \times VAF$, $0 \leq VDM \leq 1$). VDM is a measure of the goodness of an EMG decomposition that takes into account both the data approximation (VAF) and the task discrimination power (percent correct decoding) of the decomposition [18]. We computed VDM as a function of the number of temporal and spatial modules (P and N respectively) and averaged it across subjects. We then chose the values of P and N that maximized VDM. This selection ensured the inclusion of all modules that accounted for task differences and the exclusion of modules that captured task-irrelevant (noise) variations.

To compare the extracted modules with the ones obtained using other modularity models, we also implemented separate spatial decompositions [19-21] and temporal decompositions [22, 23]. We then calculated, for each subject, Pearson correlation between these modules and those obtained with the space-by-time NMF decomposition.

3) Module Clustering and Calculation of Mean Activation Coefficients

We then aimed to identify a set of modules (along with the corresponding activation coefficients) that describes muscle activations across all subjects. This could serve as a typical representation of the muscle activity of healthy participants for this experimental protocol. We therefore performed a clustering analysis and grouped modules from different subjects using a measure of similarity based on their correlation coefficients. We implemented the following procedure: 1) we sorted the modules of each subject based on which muscle they activated most (muscles were ordered as in Fig. 5); 2) we calculated the average modules across subjects and used these as reference; 3) we ordered the modules of every subject depending on their similarity (correlation coefficient) with the reference modules; 4) we clustered together modules from different subjects that had the highest similarity; 5) we averaged the modules within each cluster and we obtained the $\overline{\mathbf{w_j}}$ mean spatial and $\overline{w_i}(t)$ temporal modules; 6) we recomputed the activation coefficients for each subject with respect to $\overline{\mathbf{w_j}}$ and $\overline{w_i}(t)$ modules, according to [10].

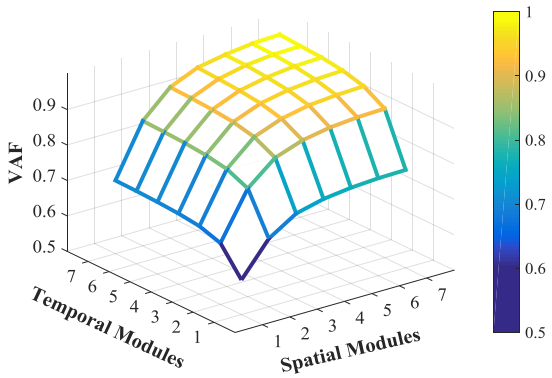

Fig. 2: Variance Accounted For as a function of the number of spatial and temporal modules. VAF expresses the goodness of EMG reconstruction from modules and activation coefficients. VAF = 1 means that the data are perfectly reconstructed. Note that a combination of 3 temporal and 4 spatial modules accounts for 93% of the EMG data variance.

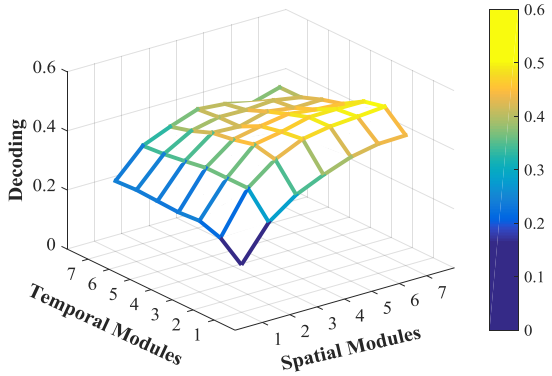

Fig. 3: Decoding performance as a function of number of modules. Shown is the fraction of correctly discriminated trials for each combination of temporal (P) and spatial (N) modules. Decoding performances > 0.41 were obtained for module combinations having $N \geq 3$ and $2 \leq P \leq 5$.

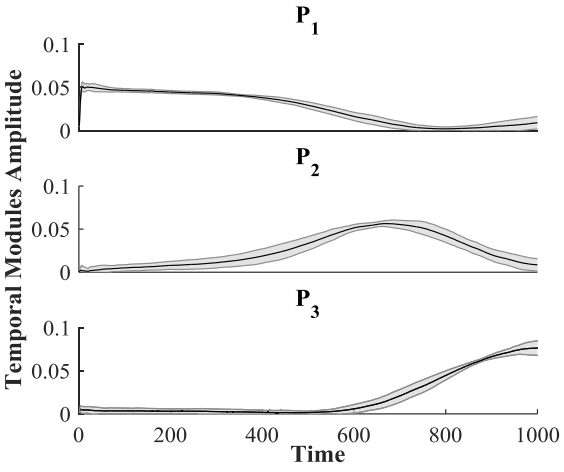

Fig. 4: Averaged temporal modules. Each subplot represents the mean (black trace) and standard deviation (grey shaded area) across subjects of temporal modules profile. Note that the three temporal modules describe muscular activation best at three different times during the movement: first activation of agonist muscles, activation of antagonist muscles and second activation of agonist muscles.

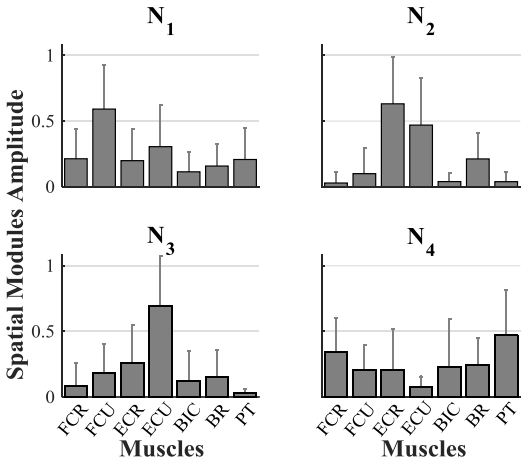

Fig. 5: Mean spatial modules across subjects. Each bar represents the mean muscular activation found in each spatial synergy. Error bars represent one standard deviation. FCR = Flexor Carpi Radialis, FCU = Flexor Carpi Ulnaris, ECR = Extensor Carpi Radialis, ECU = Extensor Carpi Ulnaris, BIC = Biceps Brachii, BR = Brachioradialis, PT = Pronator Teres.

III. RESULTS

A. Temporal and Spatial Modules Underlying Recorded Muscle Activity

To identify the spatial and temporal modules of muscle activity underlying performance of wrist movements using a robotic device, we applied the space-by-time NMF decomposition to the EMG recordings of each of the 12 subjects we tested. We first aimed to establish the numbers of temporal and spatial modules (P and N respectively) that described best the recorded muscle activity across subjects. To this end, we varied P and N (both from 1 to 7) and computed VAF and decoding performance of the modular decompositions with these numbers of modules.

We found that the average VAF across subjects showed a steady increase when P and N increased (Fig. 2). Regarding decoding performance (Fig. 3), $P \geq 3$ temporal modules maximized average percent correct decoding for any choice of N and the decoding curve saturated at $N = 3/4$. As a result, VDM was maximized for $P = 3,\ N = 4$, indicating that 3 temporal and 4 spatial modules accounted for all the task-related information of the muscle activity and any additional modules captured data-irrelevant variability, i.e. noise, in the EMG signal [13]. Hence, we selected 3 temporal and 4 spatial modules to describe muscle activity of all subjects for this set of tasks. The resulting decompositions yielded 46% correct decoding (significantly above chance, $p<10^{-4}$, chance level is 0.04) and VAF=0.93 on average across subjects.

Fig. 4 shows that the three temporal modules of the decomposition captured the tri-phasic pattern of muscular activation that is known to occur for goal-directed, discrete reaching or pointing movements [24-26]: the initial activation of agonist muscles, the following activation of antagonists to break the movement and the second agonist burst to terminate the movement at the desired target.

Fig. 5 shows the extracted spatial modules averaged across subjects. The first synergy describes the simultaneous activation of Flexor Carpi Ulnaris and Extensor Carpi Ulnaris (mainly found in adduction). The second synergy describes the co-activation of extensor muscles and Brachioradialis (mainly found in abduction), the third synergy the co-activation of extensor muscles (mainly found during extension and supination but present also in all other movements) and fourth synergy the co-activation of flexor muscles with Pronator Teres (mainly found in flexion and pronation). Biceps Brachii was almost never active.

This result can be explained as a result of the lower muscle activity required in the Passive condition which results in smaller muscle activation differences across movement directions.

B. Comparison with other Module Extraction Techniques

To validate the robustness of the identified modules irrespective of the extraction method, we separately computed P=3 temporal modules using the temporal NMF decomposition and N=4 spatial modules using the spatial NMF decomposition. We then calculated, for each subject, Pearson correlation between these modules and those obtained with the space-by-time NMF decomposition. We found that modules extracted with separate temporal and spatial decompositions were highly similar to those obtained simultaneously (0.87±0.15 and 0.73±0.11

TABLE II
CORRELATION BETWEEN INDIVIDUAL SUBJECT AND AVERAGED MODULES

	Temporal			**Spatial**			
Subject Number	**P_1**	**P_2**	**P_3**	**N_1**	**N_2**	**N_3**	**N_4**
1	0.9968*	0.9864*	0.9975*	0.8130*	0.8965*	0.9872*	0.4383
2	0.9672*	0.9932*	0.9858*	0.2276	-0.0052	0.1645	0.9654*
3	0.9781*	0.9658*	0.9924*	0.9305*	0.8180*	0.9889*	0.9206*
4	0.9830*	0.9087*	0.9650*	0.9562*	0.8979*	0.9494*	0.9001*
5	0.9970*	0.9634*	0.9942*	0.8220*	0.8498*	0.8775*	0.9584*
6	0.9978*	0.8583*	0.9954*	0.4405	0.9677*	0.7140*	0.1211
7	0.9927*	0.9975*	0.9951*	0.0159	0.9779*	0.9573*	0.7328
8	0.9891*	0.9377*	0.9839*	0.8105*	0.9801*	0.9409*	0.9326*
9	0.9699*	0.9554*	0.9870*	0.3381	0.1308	0.1635	0.7602*
10	0.9561*	0.9417*	0.9754*	-0.2859	0.7891*	0.6357	0.7896
11	0.9875*	0.9812*	0.9955*	0.5116	0.7688*	0.9534*	0.1259
12	0.9950*	0.9746*	0.9971*	0.5977	0.9433*	0.953*	0.8966*

The table shows the value of the correlation coefficient between each module of single subjects and the corresponding averaged module. Each table element reports the correlation coefficients of a given module (column) of one given subject (row). In the few cases where the correlation was poor (e.g. subjects 2 and 9) the optimal number of modules was smaller than the chosen one and therefore some of the reference modules were no represented but instead more copies of the same modules were extracted. * indicates significant correlations, p-value < 0.05.

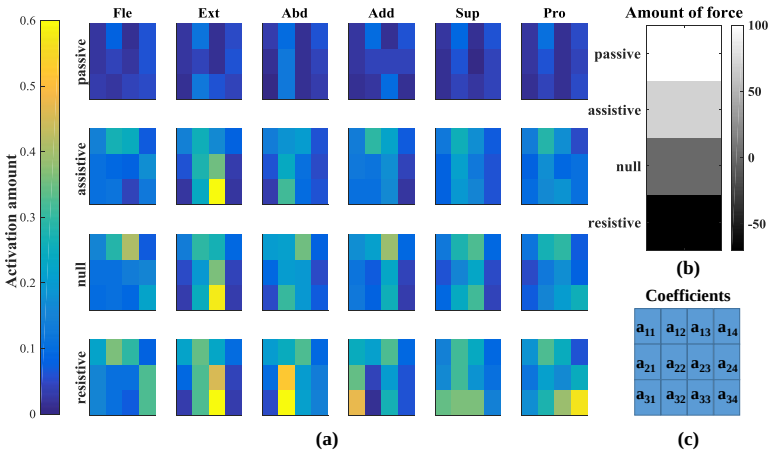

Fig. 6: Activation coefficients averaged across subjects. (a) Each panel shows the level of activation of the averaged coefficients in different task conditions and for different movements and is represented as a matrix of P = 3 rows and N = 4 columns, corresponding to the modules each coefficients is related to. Each movement (column panels) is characterized by the activation of a different set of coefficients that recruit the modules they are referred to. Coefficients also increase their value as a function of task condition (horizontal panels). (b) Amount of force field applied to each task condition. (c) Scheme to easily address the coefficients of (a). Fle = flexion, Ext = extension, Abd = abduction, Add = adduction, Sup = supination, Pro = pronation.

correlation for the temporal and spatial modules respectively, $p<0.01$). This similarity highlights the robustness of the modules reported in this study, and shows the power of the space-by-time NMF decomposition to extract - simultaneously rather than separately - robust features of EMG that describe both their spatial structure and their dynamics.

C. Correlation between Modules

To investigate whether the averaged modules were representative of each subject's muscle activation patterns, we computed correlation between a subject's modules and the corresponding averaged modules. The analysis revealed high correlation for the temporal modules and spatial modules. The individual correlations for each subject are shown in TABLE II. Mean correlation coefficient of the temporal components were $r = 0.984 \pm 0.013$ for P_1, $r = 0.955 \pm 0.039$ for P_2 and $r = 0.988 \pm 0.010$ for P_3 (significant in all cases, $p < 10^{-4}$). For the spatial modules correlations were $r = 0.514 \pm 0.387$ for N_1, $r = 0.751 \pm 0.330$ for N_2, $r = 0.773 \pm 0.305$ for N_3 and $r = 0.711 \pm 0.310$ for N_4. The correlation coefficients of the spatial modules for individual subjects (4x12 = 48 in total) ranged above 0.8 in 28 cases with $p < 0.05$, between 0.7 and 0.8 in 6 cases with $p < 0.05$ in 4 out of 6 cases, between 0.4 and 0.7 in 5 cases, and below 0.4 in the remaining 9 cases. Correlations below 0.7 were not significant.

D. Activation coefficients

The activation coefficients quantify the strength by which temporal and spatial modules are recruited in each trial in order to perform the task. Fig. 6(a) shows the average across repetitions of the same trials and across subjects of the activation coefficients calculated from the averaged modules. The activation patterns permit to discriminate across movement direction and interestingly they create complementary configurations for opposite movements along the same DoF. Extensor muscles (activated by spatial modules N_2 and N_3) are recruited in almost every movement and this is consistent with our previous finding that within the wrist robot the wrist is extended with respect to the neutral position [8] therefore activation of extensor muscles is present also in the beginning of flexion. Flexion (Fig. 6(a), first column) is characterized mainly by an activation of the second and third spatial modules (coefficients a_{12} and a_{13}) corresponding to the co-activation of extensor muscles, and it is followed, especially in the Resistive Field condition, by a second activation of the fourth spatial module (coefficients a_{24} and a_{34}) corresponding to the co-activation of Flexor Carpi Radialis and Pronator Teres. Extension (Fig. 6(a), second column) reveals a strong activation of the extensor muscles, recruited by the second and third spatial modules (mainly coefficients a_{12}, a_{23} and a_{33}). Abduction (Fig. 6(a), third column) is produced by Flexor Carpi Radialis and Extensor Carpi Radialis and indeed are recruited the second and third spatial modules involving these muscles (coefficients a_{13}, a_{22} and a_{32}). Conversely adduction (Fig. 6(a), fourth column) is produced by Flexor Carpi Ulnaris and Extensor Carpi Ulnaris and indeed starts with an activation of the third spatial module (activation of Extensor Carpi Ulnaris, coefficient a_{13}) and is followed by an activation of the first spatial modules (activation of Flexor Carpi Ulnaris, coefficient a_{21} and a_{31}). Supination (Fig. 6(a), fifth column) involves Biceps Brachii and Brachioradialis and therefore second and third spatial modules are activated by the first and third temporal modules (coefficients a_{12}, a_{13}, a_{32}, and a_{33}). Finally pronation (Fig. 6(a), sixth column) begins with activation of the extensor muscles (a_{12} and a_{13}) and terminates with Pronator Teres (coefficients a_{34}).

The level of muscular activation is naturally a function of the forces imposed by the robot. The coefficients of the space-by-time NMF decomposition captured this physiological feature, i.e. showed an increase of activation from the Passive to the Resistive Field condition (Fig.

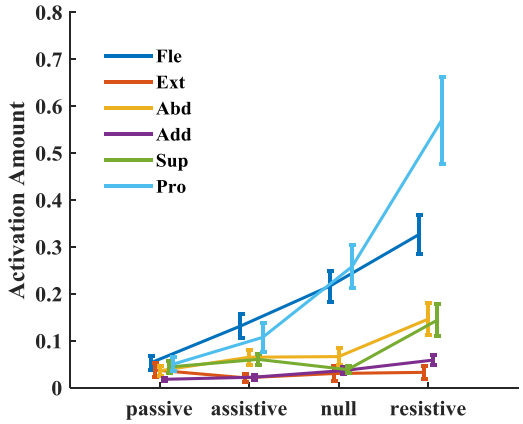

Fig. 7: Activation coefficients as a function of force modality. Shown are the mean and standard error activation value of coefficient a_{34}. Colors represent the different wrist movements. Fle = flexion, Ext = extension, Abd = abduction, Add = adduction, Sup = supination, Pro = pronation.

6(a)). Fig. 7 shows as an example, the average activation of coefficient a_{34} plotted as a function of force level, a_{34} bonded the third temporal module with the fourth spatial module, corresponding to the co-activation of Flexor Carpi Radialis and Pronator Teres. These muscles are involved in flexion and pronation and indeed, when these movements were performed, the coefficient increased with the level of force. When other movements were performed, a_{34} activation was very low.

Finally, to quantify the dependence of the activation coefficients on movement direction and force level, we decoded these two experimental variables separately. We found that both variables were discriminated significantly above chance level ($p < 10^{-4}$) which indicates that the activation coefficients captured reliably the dependence of muscle activity on both experimental factors. Percent correct decoding of force conditions (i.e. considering only trials of one given movement with different force conditions) ranged between 50%-70% for the different movement directions (decoding values: 57% ± 9% for flexion; 50% ± 14% for extension; 59% ± 22% for abduction; 63% ±16% for adduction; 70% ± 18% for supination and 59% ± 16% for pronation). Percent correct decoding of movement directions ranged between 39%-70% for the different force level conditions (decoding values: 0.39 ± 0.16 for Passive motion; 0.63 ± 0.09 for Assistive Field; 0.54 ± 0.12 for Null Field and 0.70 ± 0. 17 for Resistive Field). Movement decoding in the Passive condition was significantly lower than for the other force conditions (ANOVA test, $p < 10^{-4}$ with Assistive and Resistive condition, $p < 0.05$ with Null condition) probably because of the lower muscle activity required in the Passive condition, which results in smaller muscle activation differences across movement directions.

IV. DISCUSSION

This study examined the human muscle activation patterns underlying wrist movements under different force conditions imposed by a wrist robot. Using a space-by-time NMF decomposition method, we decomposed EMG signals into concurrent temporal and spatial modules. We then derived a set of activation coefficients that captured the recorded EMG patterns of single trials.

A combination of $P = 3$ temporal and $N = 4$ spatial modules yielded an optimal trade-off between data approximation and task discrimination while minimizing the number of modules representing the observed electromyographic activity. Variance Accounted For of the selected decomposition was 93% indicating that the resulting representation approximated accurately the recorded EMG signals. Overall decoding performance was 46% and was one order of magnitude larger than the chance level of 4%. When accounting for differences in movement directions and imposed force levels, discrimination for both factors was well above chance level, yielding decoding performance ranging between 39%-70%. This clearly indicates that the identified decomposition was able to capture information in muscle activity relating to both task variables, meaning movement direction and imposed force. Interestingly, movement direction decoding was maximal for the Resistive Field condition and minimal for the Passive Field condition. From an electrophysiological perspective, this is highly plausible, because it reflects the number of motor units recruited and their firing frequency during no or assistive force conditions, which are both necessarily lower than during a resistive force condition [27, 28]. This finding highlights that the force conditions imposed by the robot will affect motor unit recruitment and their firing frequency (rate coding), which, in turn, will affect the biofeedback signal, its decomposition and its later use as a control signal for a rehabilitation robot. The choice of $P = 3$ temporal modules matched the three different muscular activation timing patterns of agonist-antagonist bursts that characterize goal-directed arm movement [24, 25]. Moreover $N = 4$ spatial modules included all the muscular co-activations that we previously found during a similar human-robot interaction protocol [8].

The consistency between the extracted modules and those obtained using separate spatial and temporal NMF decompositions showed the effectiveness of space-by-time method in a) incorporating spatial and temporal modularity into a unique compact decomposition and b) capturing reliably the invariant (temporal and spatial) structure underlying the movements to different targets under different force conditions.

The high module correlation across subjects indicated that this structure was also shared across individuals. However, for some subjects the correlation of one or more of the 4 spatial modules was poor. This is explained by the fact that for those subjects the optimal number of spatial modules was likely to be $N < 4$. Assuming that for a given subject the spatial modules capturing all the essential information are $N = 3$ and we then impose the extraction of $N = 4$ spatial modules, the algorithm will find the three modules plus an additional one, similar to one of the first three. This last module therefore will not correlate well with the reference module to which it was paired. This caveat needs to be considered when applying the method to extract biofeedback signals that ultimately shape the force control signals of a robot interacting with a human patient.Finally, when extracting patterns of muscle activation in neurological patients, it is important to consider the notion of primary deficits and compensatory control. For example, in our recordings of healthy humans the Biceps Brachii muscle showed low activation levels, which is not surprising given that this muscle acts primarily as an elbow flexor and is typically not active during single-joint wrist movements. We here included the muscle into our analysis, because certain neurological patients such as cortical stroke survivors are known to show forearm muscle activation in order to compensate for impaired wrist muscle innervation. Indeed, it is well established that neurological disease may give rise to quite different manifestations in the electromyographic signal. For example, stroke is associated with muscular weakness affecting movement initiation and control [29], while cerebellar patients show a prolongation of agonist muscles activation and a delay of antagonist muscle activation [30]. As a result of neurological impairment, these patients may produce compensatory movements in order to minimize task errors. The selected compensatory strategy typically reflects the nature of the primary deficit and the level of initial impairment [31]. While basic muscle synergies are thought to be structured by subcortical neuronal networks and coordinated by descending cortical signals, altered

descending control due to, for example, cortical or cerebellar dysfunction will interfere with the formation of established muscle synergies [32, 33]. That is, muscles activation patterns in these patients can differ profoundly from those found on healthy subjects. Consequently, different synergies will be extracted by the described decomposition method. Thus, a comparison between the synergy modules generated by a neurologic patient and a healthy cohort can quantify the deficits in synergistic control and such information could be used to shape the robotic control signals to aid the patient.

That is, during rehabilitation, such an EMG module comparison can guide the level of assistive or resistive forces needed and when such forces shall be applied during the movement. Indeed, the use of customized robot-assisted therapy driven by EMG biofeedback has been explored and the results indicate an added rehabilitation benefit for stroke patients when compared to robotic assistance alone [34, 35]. Thus, our EMG decomposition methodology could aid the human-robot interaction by customizing robotic control signals to the motor control deficits of individual patients.

For example, the level of mismatch between healthy and pathological EMG modules resulting after one training session, could be translated into an assistive force delivered during the following training session in such a way that muscle activation more closely resembles an innervation pattern of a healthy individual. In this case the set of modules could be extracted from a small set of training trials (e.g. 5 repetitions of each task condition would be sufficient as we showed here) and this set could be used as the basis functions on which the EMG signals of each newly recorded test trial would be projected. Therefore, only $P \times N = 12$ parameters would have to be estimated. Importantly, this number does not scale with the number of muscles and/or number of recorded time points, which makes the extraction computationally inexpensive and time-efficient even for more complex and high-dimensional data.

In this scenario, the biofeedback is not presented to the patient visually to indicate errors in the timing or of the amount of muscular activation, but it is implicit and is incorporated into the human-robot control scheme. One may argue that by “hiding” the biofeedback information from the patient and embedding it into the assistance provided by the robot, the rehabilitation protocol gains the benefit of the use of the biofeedback without the drawback of user becoming frustrated by the direct observation of his/her atypical muscular activation patterns [36].

V. CONCLUSIONS

This study mapped the muscular activation of healthy individuals performing wrist movements during a motor task constrained by a robotic device. Our data show that muscle activation patterns can be reduced to a subset of stereotypical spatial and temporal patterns of muscle activation. Depending on the nature of the nervous system damage, these modules will be different for people with motor disabilities.

The reliability of the decoding and the robustness of modules across subjects indicate that the decomposition of EMG signals can be used to generate feedback signals for rehabilitation robots. This could potentially simplify and improve the motor control during training of neurologic patients.

We suggest that during motor rehabilitation of neurological patients a comparison between their abnormal synergies and those established by the age-appropriate healthy cohort can be used as a feedback signal for the control of robotic device in order to provide patient-tailored force assistance.

REFERENCES

[1] S. Masiero, E. Carraro, A. Celia, G. Rosati, and M. Armani, "Robotic therapy: a novel approach in upper-limb neurorehabilitation after stroke," Neurol Sci, vol. 28, p. 294, Oct 2007.

[2] L. Marchal-Crespo and D. J. Reinkensmeyer, "Review of control strategies for robotic movement training after neurologic injury," J Neuroeng Rehabil, vol. 6, p. 20, 2009.

[3] O. M. Giggins, U. M. Persson, and B. Caulfield, "Biofeedback in rehabilitation," J Neuroeng Rehabil, vol. 10, p. 60, 2013.

[4] J. V. Basmajian, "Biofeedback in rehabilitation: a review of principles and practices," Arch Phys Med Rehabil, vol. 62, pp. 469-75, Oct 1981.

[5] X. L. Hu, K. Y. Tong, R. Li, J. J. Xue, S. K. Ho, and P. Chen, "The effects of electromechanical wrist robot assistive system with neuromuscular electrical stimulation for stroke rehabilitation," J Electromyogr Kinesiol, vol. 22, pp. 431-9, Jun 2012.

[6] H. Huang, S. L. Wolf, and J. He, "Recent developments in biofeedback for neuromotor rehabilitation," J Neuroeng Rehabil, vol. 3, p. 11, 2006.

[7] H. I. Krebs, J. J. Palazzolo, L. Dipietro, M. Ferraro, J. Krol, K. Rannekleiv, et al., "Rehabilitation Robotics: Performance-Based Progressive Robot-Assisted Therapy," Autonomous Robots, vol. 15, pp. 7-20, 2003/07/01 2003.

[8] M. Semprini, A. Cuppone, V. Squeri, and J. Konczak, "Muscle innervation patterns for human wrist control: Useful biofeedback signals for robotic rehabilitation?," in Rehabilitation Robotics (ICORR), 2015 IEEE International Conference on, 2015, pp. 919-924.

[9] B. Cesqui, P. Tropea, S. Micera, and H. I. Krebs, "EMG-based pattern recognition approach in post stroke robot-aided rehabilitation: a feasibility study," J Neuroeng Rehabil, vol. 10, p. 75, 2013.

[10] I. Delis, S. Panzeri, T. Pozzo, and B. Berret, "A unifying model of concurrent spatial and temporal modularity in muscle activity," J Neurophysiol, vol. 111, pp. 675-93, Feb 2014.

[11] L. Masia, M. Casadio, G. Sandini, and P. Morasso, "Eye-hand coordination during dynamic visuomotor rotations," PLoS One, vol. 4, p. e7004, 2009.

[12] F. P. Kendall, Muscles: Testing and Function with Posture and Pain: Lippincott Williams & Wilkins, 2005.

[13] I. Delis, B. Berret, T. Pozzo, and S. Panzeri, "Quantitative evaluation of muscle synergy models: a single-trial task decoding approach," Front Comput Neurosci, vol. 7, p. 8, 2013.

[14] K. Yong-Deok and C. Seungjin, "Nonnegative Tucker Decomposition," in Computer Vision and Pattern Recognition, 2007. CVPR '07. IEEE Conference on, 2007, pp. 1-8.

[15] C. Alessandro, I. Delis, F. Nori, S. Panzeri, and B. Berret, "Muscle synergies in neuroscience and

robotics: from input-space to task-space perspectives," Front Comput Neurosci, vol. 7, p. 43, 2013.

[16] A. d'Avella, A. Portone, L. Fernandez, and F. Lacquaniti, "Control of fast-reaching movements by muscle synergy combinations," J Neurosci, vol. 26, pp. 7791-810, Jul 26 2006.

[17] R. Quian Quiroga and S. Panzeri, "Extracting information from neuronal populations: information theory and decoding approaches," Nat Rev Neurosci, vol. 10, pp. 173-85, Mar 2009.

[18] I. Delis, S. Panzeri, T. Pozzo, and B. Berret, "Task-discriminative space-by-time factorization of muscle activity," Front Hum Neurosci, vol. 9, p. 399, 2015.

[19] L. H. Ting and J. M. Macpherson, "A limited set of muscle synergies for force control during a postural task," J Neurophysiol, vol. 93, pp. 609-13, Jan 2005.

[20] M. C. Tresch, V. C. Cheung, and A. d'Avella, "Matrix factorization algorithms for the identification of muscle synergies: evaluation on simulated and experimental data sets," J Neurophysiol, vol. 95, pp. 2199-212, Apr 2006.

[21] M. C. Tresch, P. Saltiel, and E. Bizzi, "The construction of movement by the spinal cord," Nat Neurosci, vol. 2, pp. 162-7, Feb 1999.

[22] Y. P. Ivanenko, G. Cappellini, N. Dominici, R. E. Poppele, and F. Lacquaniti, "Coordination of locomotion with voluntary movements in humans," J Neurosci, vol. 25, pp. 7238-53, Aug 3 2005.

[23] Y. P. Ivanenko, R. E. Poppele, and F. Lacquaniti, "Five basic muscle activation patterns account for muscle activity during human locomotion," J Physiol, vol. 556, pp. 267-82, Apr 1 2004.

[24] W. J. Wadman, J. J. Denier van der Gon, R. H. Geuze, and C. R. Mol, "Control of Fast Goal-Directed Arm Movements," J Hum Mov Stud, vol. 5, pp. 3-17, 1979.

[25] M. Flanders, "Temporal patterns of muscle activation for arm movements in three-dimensional space," J Neurosci, vol. 11, pp. 2680-93, Sep 1991.

[26] E. Chiovetto, B. Berret, I. Delis, S. Panzeri, and T. Pozzo, "Investigating reduction of dimensionality during single-joint elbow movements: a case study on muscle synergies," Front Comput Neurosci, vol. 7, p. 11, 2013.

[27] C. J. De Luca and E. C. Hostage, "Relationship between firing rate and recruitment threshold of motoneurons in voluntary isometric contractions," J Neurophysiol, vol. 104, pp. 1034-46, Aug 2010.

[28] C. J. De Luca, R. S. LeFever, M. P. McCue, and A. P. Xenakis, "Behaviour of human motor units in different muscles during linearly varying contractions," J Physiol, vol. 329, pp. 113-28, Aug 1982.

[29] N. Kang and J. H. Cauraugh, "Force control improvements in chronic stroke: bimanual coordination and motor synergy evidence after coupled bimanual movement training," Exp Brain Res, vol. 232, pp. 503-13, Feb 2014.

[30] J. Hore, B. Wild, and H. C. Diener, "Cerebellar dysmetria at the elbow, wrist, and fingers," J Neurophysiol, vol. 65, pp. 563-71, Mar 1991.

[31] W. Liu, S. McCombe Waller, T. M. Kepple, and J. Whitall, "Compensatory arm reaching strategies after stroke: induced position analysis," J Rehabil Res Dev, vol. 50, pp. 71-84, 2013.

[32] V. C. Cheung, L. Piron, M. Agostini, S. Silvoni, A. Turolla, and E. Bizzi, "Stability of muscle synergies for voluntary actions after cortical stroke in humans," Proc Natl Acad Sci U S A, vol. 106, pp. 19563-8, Nov 17 2009.

[33] V. C. Cheung, A. Turolla, M. Agostini, S. Silvoni, C. Bennis, P. Kasi, et al., "Muscle synergy patterns as physiological markers of motor cortical damage," Proc Natl Acad Sci U S A, vol. 109, pp. 14652-6, Sep 4 2012.

[34] L. Dipietro, M. Ferraro, J. J. Palazzolo, H. I. Krebs, B. T. Volpe, and N. Hogan, "Customized interactive robotic treatment for stroke: EMG-triggered therapy," IEEE Trans Neural Syst Rehabil Eng, vol. 13, pp. 325-34, Sep 2005.

[35] X. L. Hu, K. Y. Tong, R. Song, X. J. Zheng, and K. H. Lui, "Robot-assisted wrist training for chronic stroke: A comparison between electromyography (EMG) driven robot and passive motion," in 2008 2nd IEEE RAS & EMBS International Conference on Biomedical Robotics and Biomechatronics, 2008, pp. 637-641.

[36] A. J. Robinson, A. J. Robinson, and L. Snyder-Mackler, Clinical Electrophysiology: Electrotherapy and Electrophysiologic Testing: Wolters Kluwer Health/Lippincott Williams & Wilkins, 2008.